Bound, even-parity $J = 0$ and $J = 2$ spectra of Sr†

Peter Esherick
IBM Thomas J. Watson Research Center, Yorktown Heights, New York 10598
(Received 16 November 1976)

Extensive new data on the even-parity, $J = 0$ and $J = 2$ states of Sr have been obtained using multiphoton ionization spectroscopy. Revised term values for previously observed $5s9d\,^1D_2$ and $^3D_2$, and $5s13d$ to $5s16d$ $^3D_2$ states are presented in addition to term values for newly observed $^1S_0$ states up to $5s21s$, $^1D_2$ states up to $5s60d$, and $^3D_2$ states up to $5s37d$. The new data clearly show an avoided crossing between the $^1D_2$ and $^3D_2$ series near the $5s16d$ levels. A strong $J = 2$ autoionizing resonance is also observed, ~ 450 cm^{-1} above the first ionization limit. Multichannel quantum-defect theory (MQDT) parametrizations of the $^1S_0$, $^1P_1^o$, $^1D_2$, and $^3D_2$ bound-state Rydberg series are also presented, including calculated term values for these series. The MQDT analysis of the $J = 2$ series in Sr differs from the earlier analysis of Ca in that both configuration interactions and recoupling between $^1D_2$ and $^3D_2$ series must be treated simultaneously. Further, it is found that all of the major perturbations of the $J = 2$ bound states can be reproduced without including any interactions due to a $4d^2\,^1D_2$, even though $3d^2\,^1D_2$ is a major perturber of the $^1D_2$ series in Ca.

I. INTRODUCTION

The addition of tunable dye lasers to the list of available light sources has allowed optical spectroscopy to expand into the realm of multiphoton processes. Of these processes, two-photon absorption has had the greatest effect on spectroscopy, since it reverses the parity selection rule of one-photon absorptions and allows transitions to occur between states of the same parity. In recent work from this laboratory, the two-photon spectrum from the $^1S_0$ ground state of calcium (Ca) was studied in considerable detail using the new technique of multiphoton ionization spectroscopy[1] (MIS). The new data obtained for $^1D_2$ and $^1S_0$ Rydberg series were then analyzed[2] using multichannel quantum-defect theory[3,4] (MQDT) to describe the extensive configuration interactions observed in the $^1D_2$ spectrum.

In this paper, the new experimental and theoretical methods used in the study[2] of Ca are applied here to the even-parity $J = 0, 2$ spectrum of the next heavier alkaline earth, strontium (Sr). Previous spectroscopic studies[5] of Sr have identified the even-parity Rydberg series $5sns\,^1S_0$ from $n = 5$ to 11, $5snd\,^1D_2$ from $n = 4$ to 9, and $5snd\,^3D$ from $n = 4$ to 12, as well as the doubly excited $5p^2\,^1S_0$ and $^1D_2$ interlopers. Although the $4d^2\,^3P$ level has been identified,[5] $^1S_0$ and $^1D_2$ states of this configuration, as well as the $4d6s\,^1D_2$ and $^3D_2$ states, have yet to be identified.

Using MIS, we have identified ten additional $5sns$ $^1S_0$ states (to $n = 21$), and over 70 additional even-parity $J = 2$ states, including the $5snd\,^1D_2$ Rydberg series to within 30 cm^{-1} of the first ionization limit. A strong $J = 2$ autoionizing resonance has also been observed ~450 cm^{-1} above the first ionization limit.

After an MQDT analysis of this data, the Sr spectrum will be compared to the previously studied Ca spectrum. The Sr $^1S_0$ spectrum closely resembles the Ca $^1S_0$ spectrum, and shows no evidence for perturbations by doubly excited configurations other than $5p^2$, which has been previously studied.[6] In the $J = 2$ spectrum, the heavier Sr atom shows an expected stronger spin-orbit coupling than Ca, which results not only in more intense transitions from the $^1S_0$ ground state to $^3D_2$ states, but also results in an observable mutual perturbation of the energy levels of the $^1D_2$ and $^3D_2$ Rydberg series.

It is found that the $J = 2$ bound-state spectrum can be accurately fit by an MQDT model which includes the recoupling of $^1D_2$ and $^3D_2$ channels, the perturbations of the $5snd\,^1D_2$ and $^3D_2$ series by $4d6s\,^1D_2$ and $^3D_2$ configurations, and the perturbation of the $^1D_2$ series by the $5p^2\,^1D_2$ configuration. Unlike the case of Ca, where the $3d^2$ configuration was important,[2] it is not necessary to include a $4d^2$ configuration to describe the $J = 2$ bound-state spectrum of Sr.

II. EXPERIMENTAL TECHNIQUES

A. Apparatus

The experimental techniques have been previously described in some detail.[2] Thus, we shall only sketch the MIS apparatus.

Strontium vapor was contained in two thermostatically controlled, heated pipes, end-fitted with fused-quartz windows. The ionization signal was detected as a current between two parallel probes which were held in the central, 30-cm-long, heated length of one pipe. A dc bias potential of 0.5 to 2.0 V was maintained between the two flat, 1×15-cm, stainless-steel probes, and a boxcar integrator was ac coupled to the negatively biased probe to detect the pulsed ion current which fol-

lowed each laser pulse.

The excitation source was a N_2 laser-pumped dye-laser/amplifier configuration. The wavelength range 428 to 465 nm was covered using mixed ethanol solutions of Eastman Coumarin 120 and 7-diethylamino-4-methyl coumarin. The dye-laser linewidth was typically 0.3 cm^{-1}. The laser power ranged from 5 to 50 kW.

The laser wavelength was calibrated, as in Ref. 2, by using the known absorption wavelengths of one-photon transitions to the $5snp\ ^1P_1^o$ odd-parity Rydberg series.[7] This was done by measuring the transmission of the second harmonic of the laser through the second (reference) pipe containing Sr vapor in a heated zone approximately 1 m in length.

The known one-photon $^1P_1^o$ spectrum was recorded on the same chart as the newly observed even-parity spectrum (observed as two-photon resonances in the ionization signal), precisely calibrating each spectral scan. Systematic errors due to pressure shifts were minimized by using the same temperature and pressure of Ne buffer gas in each pipe. No evidence of Stark mixing was observed even for applied dc fields twice as high as those used (typically ≤ 2 V/cm) in the wavelength measurements.

Figure 1 shows a spectrum taken using the typical Sr and Ne vapor pressures of 0.2 and 20 Torr, respectively. For this particular scan, the laser was circularly polarized, and only $\Delta m = \Delta J = 2$ transitions were allowed. Since the $5s^2$ ground state of Sr is of symmetry $^1S_0$, this spectrum shows only the $J=2$ states in the ionization signal.

B. Wavelength calibration procedure

The calibration procedure used in Refs. 1 and 2 was to least-squares fit observed $^1P_1^o$ absorptions to previously reported wavelengths for these transitions. We have used the same basic procedure to analyze the Sr spectra. The absorption wavelengths of the Sr $5snp\ ^1P_1^o$ series have been measured by Garton and Codling[7] (to $\pm 10^{-4}$ nm). In addition, they report a value for the first ($5s\ ^2S_{1/2}$) ionization limit of $I_s = 45\,932.0 \pm 0.2$ cm^{-1} based on their $^1P_1^o$ bound-state data. Their highest reported bound $^1P_1^o$ state, $5s33p$, lies 120 cm^{-1} below the I_s limit. In our spectra, Rydberg series can be resolved up to 30 cm^{-1} below the I_s limit, corresponding to effective quantum numbers $\nu_s \geq 60$. In order to take advantage of this new data, it was necessary to extend the $^1P_1^o$ calibration wavelengths closer to the ionization limit. This was accomplished by making an MQDT fit of the known $^1P_1^o$ term values and extrapolating beyond the $5s33p$ level. This will be described in more detail in Sec. IV. The model used a total of five adjustable parameters to fit all but the lowest two members of the reported[7] $^1P_1^o$ term values with a residual rms error of 0.12 cm^{-1}.

Table I contains the calculated $^1P_1^o$ term values that resulted from the MQDT fit to Garton and Codling's data. Use of the calculated wavelengths, rather than the experimental wavelengths of Ref. 7, resulted in ~40% improvement in the rms deviations of least-squares fits of our chart recordings of the $^1P_1^o$ absorption spectrum.

The term values reported here, in Tables III and IV, for the newly observed even-parity states were obtained after calibrating each scan via a least-squares fit to the theoretical $^1P_1^o$ wavelengths of Table I. Each reported term value represents the weighted average of from three to ten scans. The reported error bound for each weighted mean is the larger of the errors estimated from, alternatively, the scatter in the data, or the "goodness" of the calibrating fit of each scan used. These error estimates do not include any allowance for possible systematic error in the $^1P_1^o$ wavelengths[7] used here as wavelength standards. Such systematic errors, which should not affect the relative accuracy of our term values, are expected to be less than 0.2 cm^{-1}.

III. EXPERIMENTAL RESULTS

The Sr multiphoton ionization spectrum consists of a large number of one- and two-photon resonances that appear in the ionization signal as the wavelength of the excitation laser is scanned. Over the wavelength range studied, the only observed one-photon transition originating from the $5s^2\ ^1S_0$ Sr ground state was the very strong 460.7-nm resonance line, which connects the ground state to the $5s5p\ ^1P_1^o$ state. The majority of the observed resonances were two-photon transitions from the even-parity ground state to even-parity excited states. These two-photon excitations occur directly via a virtual intermediate state since the first photon was from 30 to 1300 cm^{-1} off resonance with the closest ($5s5p\ ^1P_1^o$) odd-parity state. This form of excitation has strict angular momentum selection rules. Since the initial state has $J=0$, the transitions which occur when the laser is circularly polarized are $\Delta m = \Delta J = 2$ transitions which must end in $J=2$ final states. Figure 1 shows a typical circularly polarized spectrum of even parity $J=2$ states in Sr. Alternatively, a linearly polarized laser excites both $J=0$ and $J=2$ states starting from a $J=0$ ground state. Comparison of spectra taken with these two polarizations thus allows assignment of J values.

In addition to this direct two-photon excitation process, there is also an indirect, sequential excitation process that occurs via the actual popula-

TABLE I. Calculated $^1P_1^o$ term values.

State	Expt. (cm^{-1}) [a]	Calc. (cm^{-1}) [b]	Error	ν_s(calc) [c]
$5s7p$	38 906.90	38 906.90	0.00	3.952
$4d5p$	41 172.15	41 172.15	0.00	4.801
$5s8p$	42 462.32	42 462.32	0.00	5.624
$5s9p$	43 328.04	43 328.04	0.00	6.491
$5s10p$	43 936.60	43 936.52	0.09	7.415
$5s11p$	44 366.48	44 366.60	−0.12	8.372
$5s12p$	44 675.77	44 675.85	−0.08	9.346
$5s13p$	44 903.52	44 903.57	−0.05	10.329
$5s14p$	45 075.36	45 075.36	0.00	11.317
$5s15p$	45 207.98	45 207.84	0.14	12.308
$5s16p$	45 311.87	45 312.01	−0.14	13.302
$5s17p$	45 395.47	45 395.33	0.14	14.297
$5s18p$	45 463.25	45 462.99	0.26	15.293
$5s19p$	45 518.69	45 518.66	0.03	16.290
$5s20p$	45 565.08	45 565.00	0.08	17.287
$5s21p$	45 604.04	45 603.98	0.06	18.285
$5s22p$	45 637.18	45 637.08	0.10	19.284
$5s23p$	45 665.42	45 665.42	0.00	20.282
$5s24p$	45 689.79	45 689.88	−0.08	21.281
$5s25p$	45 711.11	45 711.12	−0.01	22.280
$5s26p$	45 729.42	45 729.68	−0.26	23.279
$5s27p$	45 746.03	45 746.01	0.02	24.278
$5s28p$	45 760.22	45 760.44	−0.22	25.277
$5s29p$	45 773.27	45 773.25	0.02	26.277
$5s30p$	45 784.65	45 784.69	−0.04	27.276
$5s31p$	45 795.01	45 794.93	0.08	28.275
$5s32p$	45 804.07	45 804.14	−0.07	29.275
$5s33p$	45 812.51	45 812.46	0.05	30.275
$5s34p$		45 819.99		31.274
$5s35p$		45 826.83		32.274
$5s36p$		45 833.07		33.274
$5s37p$		45 838.77		34.273
$5s38p$		45 843.99		35.273
$5s39p$		45 848.78		36.273
$5s40p$		45 853.19		37.273
$5s41p$		45 857.27		38.272
$5s42p$		45 861.04		39.272
$5s43p$		45 864.53		40.272
$5s44p$		45 867.76		41.272
$5s45p$		45 870.78		42.272
$5s46p$		45 873.58		43.272
$5s47p$		45 876.19		44.271
$5s48p$		45 878.64		45.271
$5s49p$		45 880.93		46.271
$5s50p$		45 883.08		47.271
$5s51p$		45 885.09		48.271
$5s52p$		45 886.98		49.271
$5s53p$		45 888.76		50.271
$5s54p$		45 890.44		51.271
$5s55p$		45 892.02		52.271
$5s56p$		45 893.52		53.271
$5s57p$		45 894.93		54.270
$5s58p$		45 896.26		55.270
$5s59p$		45 897.53		56.270
$5s60p$		45 898.73		57.270

[a] Term values from Ref. 7, with the exception of the $5s7p$ value from Ref. 5.
[b] Term values calculated from the MQDT parameters in Table V.
[c] Effective quantum number relative to $^2S_{1/2}$ limit $I_s = 45\,932.19$ cm^{-1}.

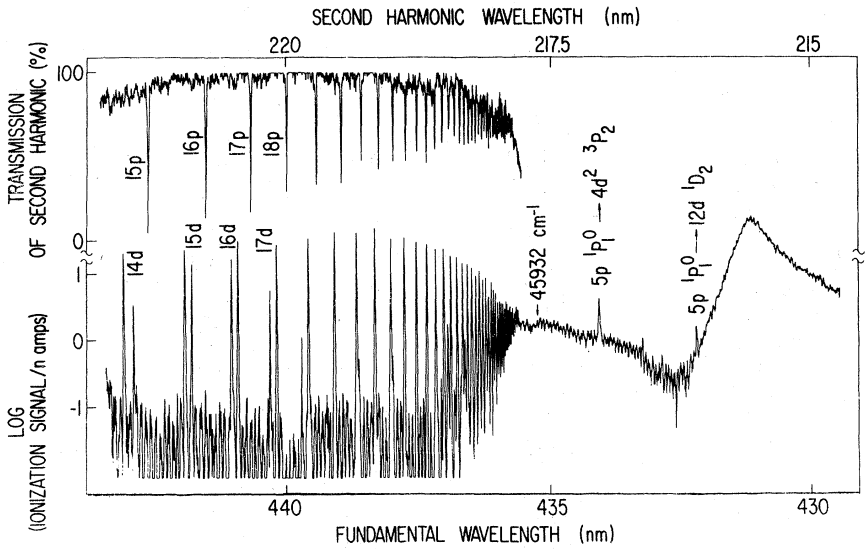

FIG. 1. Multiphoton ionization spectrum of even-parity, $J=2$ states obtained with circularly polarized laser excitation of approximately 0.2-Torr Sr (680 °C), with 20-Torr Ne buffer gas. Upper scan is the absorption, in a reference oven, of the second harmonic of the laser by the known $^1P_1^o$ Rydberg series, used for wavelength calibration.

tion of an intermediate level (usually the $5s5p\ ^1P_1^o$ state). One-photon resonances are then observed from this intermediate to higher-energy excited states. In our experiments, the intermediate state is either pumped directly in the collision broadened wings of the resonance line or indirectly via other collisional energy transfer processes. Because of the involvement of collisions, the intermediate state does not remember its m_j quantum number. Thus, in contrast to the direct two-photon excitation, no polarization effects are observed for the sequential excitations.

These one-photon resonances are easily identified, since their intensities and linewidths are strongly influenced by the buffer gas pressure and the magnitude of steady-state discharge currents between the two ionization probes. The strongest transitions of this type occurred from $5s5p\ ^1P_1^o$ to higher-energy $^1S_0$ and $^1D_2$ states, in analogy with the observations[1] in Ca. Transitions from $5s5p\ ^3P^o$ and $5s4d\ ^1D$ and ^3D terms are also observed. Table II lists the observed one-photon transitions with their respective measured and calculated energies (using Ref. 5 term values). By use of a low buffer gas pressure (~10 Torr), these collisionally induced sequential excitations can all be virtually eliminated. The remaining resonances are the direct two-photon transitions to even-parity excited states, and we shall now proceed with the analysis of this spectrum.

The $J=0$ series expected in the two-photon spectrum of Sr is primarily the $5sns\ ^1S_0$ Rydberg series which has previously been identified[5] up to 5s11s. Of the many intense two-photon transitions to $J=0$ states that we observe, the two lowest, at 43 512.0 ±0.15 and 44 096.8 ±0.15 cm^{-1} are in close agreement with the previously reported[5] term values for the 5s10s and 5s11s $^1S_0$ states. The remainder of the $J=0$ series is readily identified as $5sns\ ^1S_0$ by examination of the quantum defects, which change by less than 0.002 between the 5s10s and 5s21s states. Above 5s21s, the $^1S_0$ series is obscured by more intense transitions to $J=2$ final states, and can no longer be resolved. In addition

TABLE II. Observed one-photon resonances.

Transition	Obs. (cm^{-1})	Calc. (cm^{-1})[a]	Error
$5p\ ^1P_1^o \rightarrow 10s\ ^3S_1$	21729.0	21729.1	−0.1
$5p\ ^1P_1^o \rightarrow 10s\ ^1S_0$	21813.8	21814.1	−0.3
$5p\ ^1P_1^o \rightarrow 9d\ ^1D_2$	22057.3	22057.4[b]	−0.1
$5p\ ^1P_1^o \rightarrow 9d\ ^3D_2$	22106.5	22106.4[b]	0.1
$4d\ ^1D_2 \rightarrow 9p\ ^1P_0^o$	22312.9	22312.7	0.2
$5p\ ^1P_1^o \rightarrow 11s\ ^3S_1$	22344.9	22344.9	0.0
$5p\ ^1P_1^o \rightarrow 11s\ ^1S_0$	22398.7	22398.6	0.1
$5p\ ^3P_2^o \rightarrow 7s\ ^3S_1$	22526.2	22526.1	0.1
$5p\ ^1P_1^o \rightarrow 10d\ ^1D_2$	22543.1	22543.2[b]	−0.1
$5p\ ^1P_1^o \rightarrow 10d\ ^3D_2$	22588.6	22588.6	0.0
$5p\ ^3P_1^o \rightarrow 5p\ ^1S_0$	22655.8	22655.9	−0.1
$4d\ ^1D_2 \rightarrow 6f\ ^1F_3^o$	22689.7	22689.7	0.0
$5p\ ^1P_1^o \rightarrow 12s\ ^3S_1$	22757.8	22758.8	−1.0
$5p\ ^1P_1^o \rightarrow 12s\ ^1S_0$	22794.4	22794.3	0.1
$5p\ ^1P_1^o \rightarrow 4d^2\ ^3P_0$	22827.4	22827.4	0.0
$5p\ ^1P_1^o \rightarrow 11d\ ^1D_2$	22880.3	22880.1[b]	0.2
$5p\ ^1P_1^o \rightarrow 4d^2\ ^3P_1$?	22896.8	22897.5	−0.7
$5p\ ^3P_1^o \rightarrow 7s\ ^3S_1$?	22918.7	22920.4	−1.7
$5p\ ^1P_1^o \rightarrow 11d\ ^3D_2$	22921.2	22921.6[b]	−0.4
$5p\ ^1P_1^o \rightarrow 4d^2\ ^3P_2$	23031.0	23031.2	−0.2
$4d\ ^3D_3 \rightarrow 5f\ ^3F_4^o$	23047.4	23047.4	0.0
$5p\ ^1P_1^o \rightarrow 13s\ ^1S_0$	23074.8	23074.9	−0.1
$5p\ ^1P_1^o \rightarrow 12d\ ^1D_2$	23130.8	23129.9[b]	0.9
$4d\ ^3D_2 \rightarrow 5f\ ^3F_3^o$	23146.5	23146.7	−0.2

[a] Transition energy calculated from term values of Ref. 5, except as noted.

[b] Upper-state term value from Table IV.

to the $5sns\ ^1S_0$ series, the $(4d)^2\ ^3P_0$ state is also observed at 44 525.83, within 0.1 cm^{-1} of the value reported in Ref. 5. No other two-photon transitions to $J=0$ final states were observed. Table III summarizes the observed $J=0$ term values.

Aside from a $(4d)^2\ ^3P_2$ state, which had already been identified, the newly observed $J=2$ states fall into two Rydberg series, namely $^1D_2$ and $^3D_2$, both converging on the first ionization limit. By analogy with Ca, both the $5snd\ ^1D_2$ and $^3D_2$ series should be perturbed by $4d6s$ interlopers, and the $^1D_2$ series may also be perturbed by a $4d^2$ interloper. In addition to the effects of these interlopers, there is the possibility of mixing between the $^1D_2$ and $^3D_2$ channels if LS coupling breaks down.

The more intense of the observed $J=2$ series, the $5snd\ ^1D_2$, has previously been reported[5] up to the $5s9d$ state. Although our data are in agreement with Ref. 5 on the $5s8d\ ^1D_2$ state at 43 020.9 cm^{-1} we do not see any peak in the multiphoton ionization spectra at the 43 780.6 cm^{-1} energy previously assigned[5] to $5s9d\ ^1D_2$. However, a strong peak is observed in our spectra at 43 755.9 cm^{-1}. Thus, the $5s9d\ ^1D_2$ state of Sr has been misassigned in Ref. 5, similar to the earlier misassignment of $4s7d\ ^1D_2$ in Ca (see Ref. 2). In Sec. IV D we shall show that all of the intense $J=2$ states that we do observe form a reasonable Rydberg series extending from the previously known[5] $5s4d$-$5s8d\ ^1D_2$ levels.

The $5snd\ ^3D$ series has been reported up to $5s16d$, with the $J=2$ term ($^3D_2$) unresolved. This series matches quite well with the weaker intensity

TABLE III. Observed and calculated $^1S_0$ bound series.

Label	Obs. (cm^{-1})	Calc. (cm^{-1})[a]	Error	ν_s(Obs.)	ν_s(calc.)
$5s6s$	30 591.80[b]	c		2.675	
$5p^2$	37 160.28[b]	37 160.32	−0.04	3.537	3.537
$5s7s$	38 444.05[b]	38 443.97	0.09	3.828	3.828
$5s8s$	41 052.50[b]	41 053.03	−0.53	4.742	4.742
$5s9s$	42 596.00[b]	42 596.27	−0.27	5.735	5.735
$5s10s$	43 512.00 ±0.18	43 511.87	0.14	6.734	6.733
$5s11s$	44 096.84 ±0.17	44 096.94	−0.10	7.732	7.733
$5s12s$	44 492.83 ±0.18	44 493.06	−0.22	8.732	8.732
$4d^2\ ^3P_0$	44 525.83 ±0.11	c		8.833	
$5s13s$	44 773.36 ±0.11	44 773.55	−0.19	9.731	9.732
$5s14s$	44 979.25 ±0.16	44 979.39	−0.14	10.731	10.732
$5s15s$	45 134.88 ±0.11	45 134.88	0.00	11.732	11.732
$5s16s$	45 255.31 ±0.10	45 255.20	0.11	12.733	12.732
$5s17s$	45 350.35 ±0.07	45 350.21	0.15	13.733	13.732
$5s18s$	45 426.52 ±0.07	45 426.53	−0.01	14.731	14.732
$5s19s$	45 488.74 ±0.07	45 488.77	−0.04	15.731	15.732
$5s20s$	45 540.10 ±0.07	45 540.19	−0.09	16.730	16.732
$5s21s$	45 583.18 ±0.12	45 583.16	0.02	17.732	17.732
$5s22s$		45 619.43			18.732
$5s23s$		45 650.33			19.731
$5s24s$		45 676.86			20.731
$5s25s$		45 699.82			21.731
$5s26s$		45 719.82			22.731
$5s27s$		45 737.34			23.731
$5s28s$		45 752.78			24.731
$5s29s$		45 766.45			25.731
$5s30s$		45 778.62			26.731
$5s31s$		45 789.49			27.731
$5s32s$		45 799.25			28.731
$5s33s$		45 808.05			29.731
$5s34s$		45 815.99			30.731
$5s35s$		45 823.20			31.731
$5s36s$		45 829.76			32.731
$5s37s$		45 835.74			33.731
$5s38s$		45 841.22			34.731
$5s39s$		45 846.24			35.731
$5s40s$		45 850.85			36.731

[a] Calculated using MQDT parameters given in Table VI.
[b] Reference 5.
[c] This state not included in MQDT fit.

$J=2$ states observed in the multiphoton ionization spectrum. The agreement with Ref. 5 is very good for the resolved $5s10d$-$5s12d$ $^3D_2$ term values; however, we suggest new term values for the $5s9d$ $^3D_2$ and those higher $^3D_2$ terms which have not been previously resolved. The newly observed $^3D_2$ levels will also be shown, in Sec. IV D, to form a reasonable Rydberg series connecting with the previously resolved $^3D_2$ terms.

Table IV summarizes the measured term values for all of the observed $J=2$ states. The nominal $5snd$ labels of Ref. 5 have been continued, sequentially in n, for the new term values for the convenience of identifying levels.

In addition to the $J=0$ and $J=2$ bound state series, a strong autoionizing resonance is also observed in the multiphoton ionization spectrum (Fig. 1). Polarization experiments indicate that the resonance corresponds to a $J=2$ state. The observed asymmetric line shape, which is due to interference between the $J=2$ continuum and autoionizing state oscillator strengths, supports the assignment of the resonance to a $J=2$ state of Sr. The peak intensity occurs at 46380 cm^{-1}, 450 cm^{-1} above the first ionization limit. Although broad in comparison to bound-state resonances, the 60 cm^{-1} (FWHM) linewidth of this resonance is actually quite sharp, particularly for the lowest member of an autoionizing series. The possible assignment of this resonance as the $4d^2$ $^1D_2$ state of Sr will be discussed at the end of Sec. IV D.

IV. MULTICHANNEL QUANTUM DEFECT THEORY

A. Introduction

The observed spectra will be interpreted in this section, closely following Ref. 2. We begin with an abbreviated review of the basis for an MQDT analysis, as previously developed in Refs. 8 and 9.

The MQDT relies on the fact that at distances r greater than some radius r_0 from an ion core, an (outer) electron moves in a very nearly Coulombic potential. In this region, $r>r_0$, the wave function can be analytically described as a superposition of "dissociation" or "collision" channels. Each such channel (i) is labeled by the state of the ion core, the state of the outer electron, and their coupling. Associated with each channel (i) is an effective quantum number ν_i which is a function of energy E given by the Rydberg formula:

$$E=I_i-R/\nu_i^2 \tag{1a}$$

or

$$\nu_i=[R/(I_i-E)]^{1/2}, \tag{1b}$$

where R is the mass-corrected Rydberg constant and I_i is the ionization limit corresponding to the state of the ion core in the ith collision channel. The combined solution of Eq. (1b) for all ν_i as a function of E traces out a line $\mathcal{L}$ in the multidimensional space of the ν_i's.

A different basis set is obtained by considering the scattering matrix S and its diagonalization. The matrix $U_{i\alpha}$, which diagonalizes S with eigenvalues $e^{2\pi i\mu_\alpha}$, provides the transformation between the i collision channels and a set of Ψ_α "eigenchannels" which describe the short-range effects of the many-electron interactions for the region $r<r_0$.

The eigenstates of the system are found by applying the appropriate boundary conditions at $r\to\infty$. This leads to equations of the form:

$$\sum_\alpha U_{i\alpha}\sin\pi(\nu_i+\mu_\alpha)A_\alpha=0 \quad \text{for all } i \tag{2}$$

where the A_α are the coefficients of the eigenfunction in the Ψ_α basis. The nontrivial solution of Eq. (2) requires that

$$\mathrm{Det}\left|U_{i\alpha}\sin\pi(\nu_i+\mu_\alpha)\right|=0. \tag{3}$$

Since the various ν_i's appearing in the above equation, which describes a surface $\mathcal{S}$, are all interrelated via Eq. (1), the energies of the bound eigenstates can be found by simultaneously satisfying Eqs. (1) and (3), i.e., at the intersection of the curve $\mathcal{L}$ and the surface $\mathcal{S}$. Analysis of a spectrum thus consists of adjusting the μ_α and $U_{i\alpha}$ so that the term values given by Eqs. (1) and (3) agree with the experimental data.

In addition to providing a means of fitting experimentally determined eigenstate energies, MQDT also provides detailed information on the extent of configuration mixing that occurs in these eigenstates. Although the Ψ_α eigenchannels are, in general, mixed configurations, the i collision channels are all pure configurations. The admixture of configurations is thus given by Eq. (2.11) of Ref. 9:

$$Z_i^{(n)}=(-1)^{(l_i+1)}\nu_i^{3/2}\sum_\alpha U_{i\alpha}\cos\pi(\nu_i^{(n)}+\mu_\alpha)A_\alpha^{(n)}/N_n \tag{4}$$

where $Z_i^{(n)}$ is the coefficient of the ith collision channel in the nth eigenstate, $\Psi^{(n)}$, and N_n is a normalization factor.[9]

B. Analysis of the bound $^1P_1^o$ spectrum

The absorption wavelengths of the Sr $5snp$ $^1P_1^o$ series, up to $5s33p$, have been previously mea-

TABLE IV. Observed and calculated bound, even-parity, $J=2$ series.

Nomin. Label	Obs. (cm^{-1})	Calc. (cm^{-1}) [a]	Error	ν_s(expt.)	ν_s(calc)
$5s5d\ ^1D_2$	34727.48 [b]	34728.06	−0.58	3.129	3.130
$5s5d\ ^3D_2$	35022.02 [b]	c		3.171	
$5p^2\ ^1D_2$	36960.88 [b]	36960.64	0.24	3.497	3.497
$5s6d\ ^3D_2$	39690.85 [b]	36691.11	−0.26	4.193	4.193
$5s6d\ ^1D_2$	39733.11 [b]	39736.04	−2.93	4.207	4.208
$5s7d\ ^1D_2$	41831.70 [b]	41828.83	2.87	5.173	5.171
$5s7d\ ^3D_2$	41869.32 [b]	41867.66	1.66	5.197	5.196
$5s8d\ ^1D_2$	43020.90 [b]	43019.69	1.21	6.139	6.138
$5s8d\ ^3D_2$	43070.31 [b]	43070.16	0.15	6.192	6.192
$5s9d\ ^1D_2$	43755.88 ±0.15	43755.74	0.14	7.101	7.101
$5s9d\ ^3D_2$	43804.89 ±0.22	43805.33	−0.44	7.182	7.183
$5s10d\ ^1D_2$	44241.70 ±0.11	44242 39	−0.69	8.057	8.059
$5s10d\ ^3D_2$	44287.05 ±0.20	44287.54	−0.49	8.167	8.168
$5s11d\ ^1D_2$	44578.58 ±0.11	44581.33	−2.75	9.004	9.013
$5s11d\ ^3D_2$	44620.08 ±0.16	44620.59	−0.51	9.145	9.147
$4d^2\ ^3P_2$	44729.56 ±0.11	c		9.552	
$5s12d\ ^1D_2$	44829.40 ±0.11	44827.26	2.14	9.975	9.966
$5s12d\ ^3D_2$	44860.28 ±0.20	44859.82	0.46	10.118	10.116
$5s13d\ ^1D_2$	45011.77 ±0.11	45011.57	0.20	10.919	10.918
$5s13d\ ^3D_2$	45036.85 ±0.11	45036.93	−0.08	11.071	11.071
$5s14d\ ^1D_2$	45153.10 ±0.11	45153.14	−0.04	11.868	11.868
$5s14d\ ^3D_2$	45171.54 ±0.13	45171.40	0.14	12.011	12.010
$5s15d\ ^{1,3}D_2$	45263.62 ±0.14	45263.57	0.05	12.812	12.811
$5s15d\ ^{1,3}D_2$	45276.62 ±0.12	45276.49	0.13	12.938	12.937
$5s16d\ ^{1,3}D_2$	45350.35 ±0.07	45350.47	−0.12	13.733	13.735
$5s16d\ ^{1,3}D_2$	45362.03 ±0.06	45361.98	0.05	13.873	13.873
$5s17d\ ^3D_2$	45420.78 ±0.07	45420.80	−0.02	14.648	14.649
$5s17d\ ^1D_2$	45433.14 ±0.08	45433.16	−0.02	14.829	14.829
$5s18d\ ^3D_2$	45479.88 ±0.07	45479.87	0.01	15.576	15.576
$5s18d\ ^1D_2$	45492.48 ±0.06	45492.53	−0.05	15.798	15.799
$5s19d\ ^3D_2$	45530.17 ±0.08	45530.21	−0.04	16.522	16.522
$5s19d\ ^1D_2$	45542.12 ±0.06	45542.24	−0.12	16.773	16.775
$5s20d\ ^3D_2$		45573.23			17.485
$5s20d\ ^1D_2$	45584.17 ±0.06	45584.15	0.02	17.757	17.757
$5s21d\ ^3D_2$		45610.08			18.458
$5s21d\ ^1D_2$	45619.60 ±0.06	45619.76	−0.16	18.737	18.741
$5s22d\ ^3D_2$	45641.68 ±0.07	45641.75	−0.07	19.436	19.438
$5s22d\ ^1D_2$	45650.26 ±0.08	45650.24	0.02	19.729	19.728
$5s23d\ ^3D_2$	45669.14 ±0.10	45669.09	0.05	20.425	20.423
$5s23d\ ^1D_2$	45676.51 ±0.06	45676.52	−0.01	20.717	20.717
$5s24d\ ^3D_2$	45692.81 ±0.07	45692.82	−0.01	21.411	21.411
$5s24d\ ^1D_2$	45699.25 ±0.06	45699.32	−0.07	21.705	21.708
$5s25d\ ^3D_2$	45713.51 ±0.07	45713.53	−0.02	22.401	22.402
$5s25d\ ^1D_2$	45719.25 ±0.06	45719.23	0.02	22.701	22.700
$5s26d\ ^3D_2$	45731.80 ±0.07	45731.69	0.11	23.401	23.395
$5s26d\ ^1D_2$	45736.80 ±0.06	45736.71	0.09	23.699	23.693
$5s27d\ ^3D_2$	45747.81 ±0.07	45747.70	0.11	24.396	24.389
$5s27d\ ^1D_2$	45752.22 ±0.06	45752.13	0.09	24.693	24.687
$5s28d\ ^3D_2$		45761.88			25.384
$5s28d\ ^1D_2$	45765.79 ±0.06	45765.81	−0.02	25.680	25.682
$5s29d\ ^3D_2$	45774.58 ±0.07	45774.50	0.08	26.387	26.380
$5s29d\ ^1D_2$	45777.98 ±0.06	45777.99	−0.01	26.676	26.677
$5s30d\ ^3D_2$	45785.87 ±0.07	45785.77	0.10	27.386	27.376
$5s30d\ ^1D_2$	45788.90 ±0.06	45788.89	0.01	27.674	27.673
$5s31d\ ^3D_2$	45795.91 ±0.07	45795.88	0.03	28.377	28.373
$5s31d\ ^1D_2$	45798.65 ±0.06	45798.78	−0.02	28.666	28.669
$5s32d\ ^3D_2$	45805.02 ±0.07	45804.98	0.04	29.376	29.371
$5s32d\ ^1D_2$	45807.46 ±0.06	45807.50	−0.03	29.662	29.666
$5s33d\ ^3D_2$	45813.18 ±0.09	45813.20	−0.02	30.366	30.368

TABLE IV. (*Continued*)

Nomin. Label	Obs. (cm^{-1})	Calc. (cm^{-1})[a]	Error	ν_s(expt.)	ν_s(calc)
$5s33d\ ^1D_2$	45 815.60 ±0.09	45 815.47	0.13	30.680	30.663
$5s34d\ ^3D_2$	45 820.69 ±0.09	45 820.65	0.04	31.372	31.366
$5s34d\ ^1D_2$	45 822.71 ±0.06	45 822.71	0.00	31.660	31.660
$5s35d\ ^3D_2$	45 827.55 ±0.09	45 827.42	0.13	32.384	32.364
$5s35d\ ^1D_2$	45 829.32 ±0.06	45 829.30	0.02	32.662	32.658
$5s36d\ ^3D_2$	45 833.54 ±0.12	45 833.60	−0.06	33.353	33.363
$5s36d\ ^1D_2$	45 835.30 ±0.06	45 835.31	−0.01	33.654	33.655
$5s37d\ ^3D_2$	45 839.32 ±0.12	45 839.25	0.07	34.375	34.361
$5s37d\ ^1D_2$	45 840.85 ±0.07	45 840.81	0.04	34.662	34.653
$5s38d\ ^3D_2$		45 844.42			35.360
$5s38d\ ^1D_2$	45 845.91 ±0.07	45 845.85	0.06	35.664	35.651
$5s39d\ ^3D_2$		45 849.18			36.359
$5s39d\ ^1D_2$	45 850.53 ±0.07	45 850.49	0.04	36.659	36.650
$5s40d\ ^3D_2$		45 853.56			37.358
$5s40d\ ^1D_2$	45 854.83 ±0.07	45 854.77	0.06	37.664	37.648
$5s41d\ ^3D_2$		45 857.60			38.357
$5s41d\ ^1D_2$	45 858.75 ±0.07	45 858.72	0.04	38.656	38.647
$5s42d\ ^3D_2$		45 861.34			39.356
$5s42d\ ^1D_2$	45 862.44 ±0.07	45 862.37	0.07	39.665	39.645
$5s43d\ ^3D_2$		45 864.80			40.355
$5s43d\ ^1D_2$	45 865.84 ±0.07	45 865.76	0.08	40.669	40.644
$5s44d\ ^3D_2$		45 868.02			41.355
$5s44d\ ^1D_2$	45 869.01 ±0.07	45 868.91	0.10	41.677	41.643
$5s45d\ ^3D_2$		45 871.01			42.354
$5s45d\ ^1D_2$	45 871.91 ±0.07	45 871.84	0.08	42.671	42.642
$5s46d\ ^3D_2$		45 873.80			43.353
$5s46d\ ^1D_2$	45 874.61 ±0.07	45 874.57	0.04	43.657	43.641
$5s47d\ ^3D_2$		45 876.40			44.353
$5s47d\ ^1D_2$	45 877.10 ±0.07	45 877.12	−0.02	44.632	44.640
$5s48d\ ^3D_2$		45 878.83			45.352
$5s48d\ ^1D_2$	45 879.51 ±0.07	45 879.50	0.01	45.642	45.639
$5s49d\ ^3D_2$		45 881.11			46.352
$5s49d\ ^1D_2$	45 881.76 ±0.07	45 881.74	0.02	46.649	46.638
$5s50d\ ^3D_2$		45 883.24			47.351
$5s50d\ ^1D_2$	45 883.83 ±0.07	45 883.83	0.00	47.637	47.638
$5s51d\ ^1D_2$	45 885.75 ±0.07	45 885.80	−0.05	48.612	48.637
$5s52d\ ^1D_2$	45 887.61 ±0.07	45 887.65	−0.04	49.616	49.636
$5s53d\ ^1D_2$	45 889.38 ±0.07	45 889.39	−0.01	50.631	50.636
$5s54d\ ^1D_2$	45 891.03 ±0.07	45 891.03	0.00	51.636	51.635
$5s55d\ ^1D_2$	45 892.59 ±0.07	45 892.58	0.01	52.643	52.635
$5s56d\ ^1D_2$	45 894.04 ±0.07	45 894.04	0.00	53.635	53.634
$5s57d\ ^1D_2$	45 895.39 ±0.07	45 895.42	−0.03	54.610	54.634
$5s58d\ ^1D_2$	45 896.74 ±0.07	45 896.73	0.01	55.640	55.633
$5s59d\ ^1D_2$	45 898.01 ±0.07	45 897.97	0.04	56.664	56.633
$5s60d\ ^1D_2$	45 899.20 ±0.07	45 899.15	0.05	57.677	57.632
$5s61d\ ^1D_2$		45 900.27			58.632
$5s62d\ ^1D_2$		45 901.33			59.632
$5s63d\ ^1D_2$		45 902.34			60.631
$5s64d\ ^1D_2$		45 903.30			61.631
$5s65d\ ^1D_2$		45 904.21			62.631
$5s66d\ ^1D_2$		45 905.08			63.630
$5s67d\ ^1D_2$		45 905.92			64.630
$5s68d\ ^1D_2$		45 906.71			65.630
$5s69d\ ^1D_2$		45 907.47			66.630
$5s70d\ ^1D_2$		45 908.19			67.629

[a] Calculated using MQDT parameters given in Table VII.
[b] Reference 5.
[c] This state not included in MQDT fit.

sured,[7] and have been used in this work as wavelength standards. The following MQDT analysis of the $^1P_1^o$ term values of Ref. 7 was carried out in order to obtain (1) more accurate term values for the previously observed $^1P_1^o$ states and (2) additional calibration wavelengths corresponding to $5snp$ $^1P_1^o$ states above $5s33p$. These goals were met by least-squares fitting the $^1P_1^o$ term values of Ref. 7 to a two-channel MQDT model. The effects of random experimental error in the measured[7] $^1P_1^o$ term values were reduced by using term values calculated from this least-squares fit for the wavelength calibration. Extrapolation of the MQDT model to higher energies than $5s33p$ then allowed calculation of $^1P_1^o$ term values as close to the $(5s)$ ionization limit as desired. An improved value for the $5s(^2S_{1/2})$ ionization limit was also obtained from this MQDT fit.

Since the only rigorous quantum numbers are J and parity, a rigorous treatment of the $^1P_1^o$ bound states should include all odd-parity $J=1$ states. For the bound-state energies of Sr, this set includes $^1P_1^o$ and $^3P_1^o$ Rydberg series of $5snp$ configurations, and $^1P_1^o$, $^3P_1^o$, and $^3D_1^o$ terms of the $4d5p$ doubly excited configuration. In practice, however, it is found that L and S are sufficiently good quantum numbers that the $^1P_1^o$ bound state data can be treated independently of $^3P_1^o$ and $^3D_1^o$ terms. We thus consider only the interaction of the $5snp$ $^1P_1^o$ series with the $4d5p$ $^1P_1^o$ interloper.

The first step of any MQDT treatment is to define the relevant collision channels and to determine the appropriate ionization limits I_i for each of these channels. Equation (1) then defines an effective quantum number ν_i for each value of I_i. (Note that in a many channel treatment, where several series may converge on the same ionization limit, not all of the I_i, and thus not all of the ν_i, are distinct).

The $5snp$ $^1P_1^o$ series converges on the $5s$ $^2S_{1/2}$ ionization limit, and thus, the effective quantum number $\nu_i \equiv \nu_s$ for this channel is given by using the limit $I_i \equiv I_s = 45\,932.0$ cm^{-1} (from Ref. 7) in Eq. (1). The appropriate choice of limit for the $4dnp$ $^1P_1^o$ channel (of which the $4d5p$ interloper is the lowest member) is more difficult since this series mixes with $4dnp$ $^3P_1^o$ and $^3D_1^o$ series. The resulting recoupled series converge onto spin-orbit split $4d$ $^2D_{3/2}$ and $^2D_{5/2}$ limits at 60 488 and 60 768 cm^{-1}, respectively.[7] Both of these limits are important in a more complete MQDT treatment, where all of these channels are treated together and the recoupling from LS to jj coupling near these limits is handled explicitly. However, for the simplified treatment of $^1P_1^o$ bound states, it will suffice to use the average value $I_d = 60628$ cm^{-1} to determine the ν_d effective quantum number.

With the above choice of two collision channels for this MQDT model, the parametrization of the bound state requires (1) the fitting of a 2×2 unitary matrix $U_{i\alpha}$ which transforms these (i) collision channels into close-coupled (α) eigenchannels, and (2) the fitting of two μ_α eigendefects. This constitutes the minimum set of three independent parameters for a two-channel MQDT model. These parameters may, in general, be (analytic) functions of the energy[9] E, which may increase the number of parameters required to accurately fit the data.

The procedure used to fit the $^1P_1^o$ data[7] was identical to that used in Ref. 2, and was used for all data fitting in this paper. Initial estimates of parameters were obtained by inspection of a quantum-defect plot, and adjustments of these parameters were made following graphical comparison of the theory with the measured quantum defects. Parameters obtained in this manner were refined by least-squares fitting the measured term values to term values calculated from the MQDT parametrization.

Figure 2(a) is a plot of the quantum defects (ν_s versus ν_d, modulo 1) of the $^1P_1^o$ bound states. The solid line, S, represents the solution of Eq. (2) using the best fit parameters obtained for this series. This fit has used one (linearly) energy-dependent eigendefect, which was found to greatly improve the fit of the lower-energy $^1P_1^o$ states. For these lower-energy states, polarization of the ion core by the outer electron introduces appreciable energy dependence into the MQDT parameters.[2] Thus, even though the $5s6p$ $^1P_1^o$ energy is fit quite well with this model, this level and the next lower ($5s5p$ $^1P_1^o$) level were excluded from the least-squares fit in order to maximize the accuracy of the fit at higher energies where core polarization is less important.

An expanded quantum-defect plot of the $^1P_1^o$ data and the MQDT fit near the I_s limit is shown in Fig. 3(a). Although the two-channel theoretical fit predicts a non zero slope of the quantum-defect curve, due to the extensive perturbative influence of the $4d5p$ state, the plot of the data[7] using the value $I_s = 45932.0$ cm^{-1} from Ref. 7 is seen to scatter about a more nearly horizontal line. This would be expected if the value for I_s had been chosen on the assumption that the quantum defects for the states $5s22p$ to $5s33p$ should be nearly constant. Since MQDT shows that this is not necessarily a valid assumption, the ionization limit I_s was added to the adjustable parameters in the MQDT fit, which was then repeated. (Note that the effect of any additional perturbing channels would be to deflect the quantum defect curve up rather than down, towards horizontal).

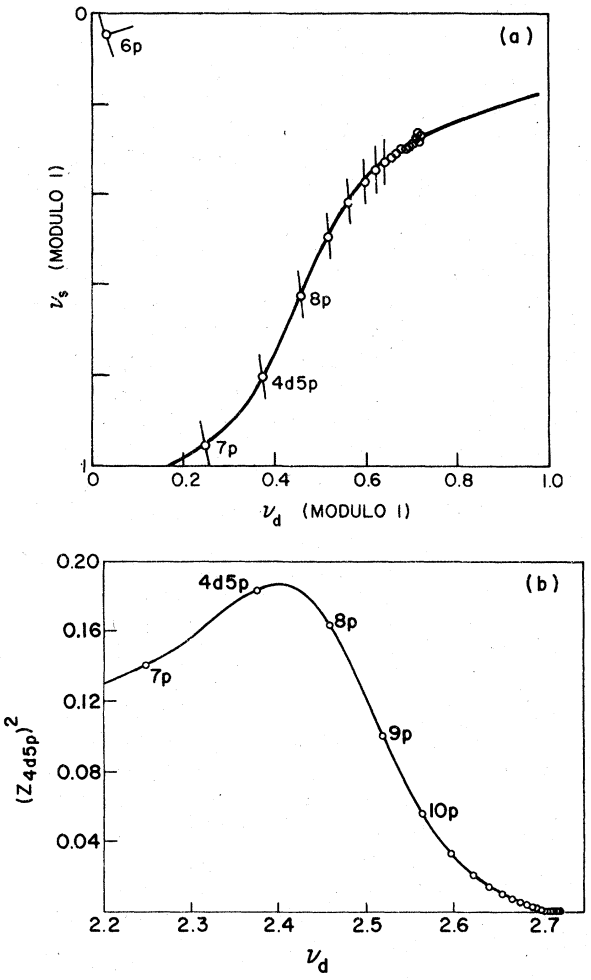

FIG. 2. (a) Quantum-defect plot of the bound $^1P_1^o$ data of Ref. 7. The solid line is the curve $\mathcal{S}$ given by solving Eq. (3) with the MQDT parameters in Table V using the ionization limits $I_s = 45\,932.19$ cm^{-1} and $I_d = 60\,628.27$ cm^{-1}. The short, vertical lines are sections of the curve $\mathcal{L}$ [Eq. (1)]. (b) Admixture of the $4d5p$ configuration in the bound $^1P_1^o$ spectrum, calculated from Eq. (4) with the MQDT parameters in Table V.

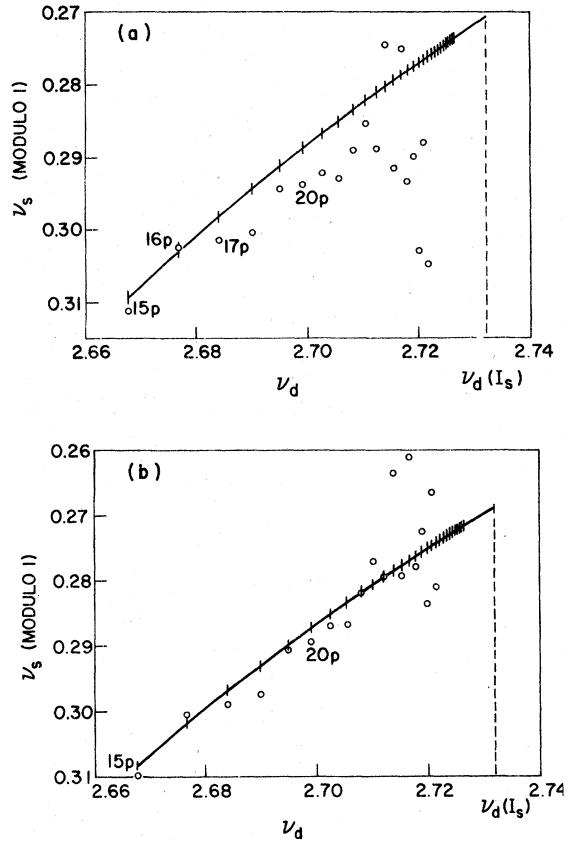

FIG. 3. Expanded quantum-defect plot of the $^1P_1^o$ data of Ref. 7 near the first, $5s\ ^2S_{1/2}$, ionization limit I_s. (a) Plot of the data (Ref. 7) and theoretical fit (solid line) using $I_s = 45932.0$ cm^{-1} from Ref. 7. (b) Result of theoretical fit allowing adjustment of the I_s limit. Plot obtained using the new value $I_s = 45\,932.19$ cm^{-1}. Calculated eigenstates are found at the intersections of the solid curve $\mathcal{S}$ [Eq. (3)] with the short, nearly vertical, lines $\mathcal{L}$ which are sections of the curve given by Eq. (1).

The complete set of parameters obtained from this least-squares fit is presented in Table V. Figure 3(b) is the corresponding quantum-defect plot of both the data and the theoretical fit, plotted using the revised value of $I_s = 45\,932.19 \pm 0.03$ cm^{-1} plus possible systematic errors ≤ 0.2 cm^{-1}. Table I lists term values calculated using the above model and extrapolated up to the $5s60p$ level. The rms error between the observed and calculated term values is 0.12 cm^{-1}.

Figure 2(b) presents the percentage admixture $(Z_{4d5p})^2$, given by Eq. (4) of the $4d5p$ configuration in the $^1P_1^o$ Rydberg series using the MQDT param-

TABLE V. MQDT parameters for the $^1P_1^o$ bound states.

$i, \alpha = 1$	2
$\lvert i\rangle = 5snp$	$4dnp$
$I_i = 45\,932.19$	60 628.26
$\mu_\alpha = 0.8936(4)$ [a]	0.49059(3)
$\frac{d\mu_\alpha}{dE} = 0.249(2)$ [b]	0
$U_{1\alpha} = 0.8172(1)$	−0.5763(1)

[a] Probable error in last digit shown in parentheses.

[b] Normalized to energy from ground state to first (I_s) limit.

eters of Table V. The maximum admixture of 18% occurs for the level at 41172 cm^{-1} labeled as $4d5p$ by Ref. 7; however, this configuration is seen to be spread out over several members of the $^1P_1^o$ series. The sum of the $(Z_{4d5p})^2$ over all the bound states from $5s6p$ up is 0.89, with the remainder presumably mixed in the $5s5p$ state. This lowest member of the series is poorly treated by MQDT, not only because of the core polarization problems discussed above, but also for reasons described in the discussion section of Ref. 2.

C. Analysis of the bound $^1S_0$ spectrum

An MQDT analysis of the Sr bound $^1S_0$ spectrum,[5] up to $5s11s$ $^1S_0$, was presented by Lu in his study[6] of the effects of $(np)^2$ terms on the spectra of alkaline earths. Although the new data presented here provide term values for ten additional $^1S_0$ bound states (up to $5s21s$), they provide no evidence for any new additional perturbing channels. In particular, there is no evidence of perturbations by a $4d^2$ $^1S_0$ state. Thus, the earlier two-channel ($5sns$ and $4p^2$) analysis by Lu remains valid. In this section, we report refined parameters for the above MQDT model obtained from the least-squares fit of the combined data from this work and from Ref. 5.

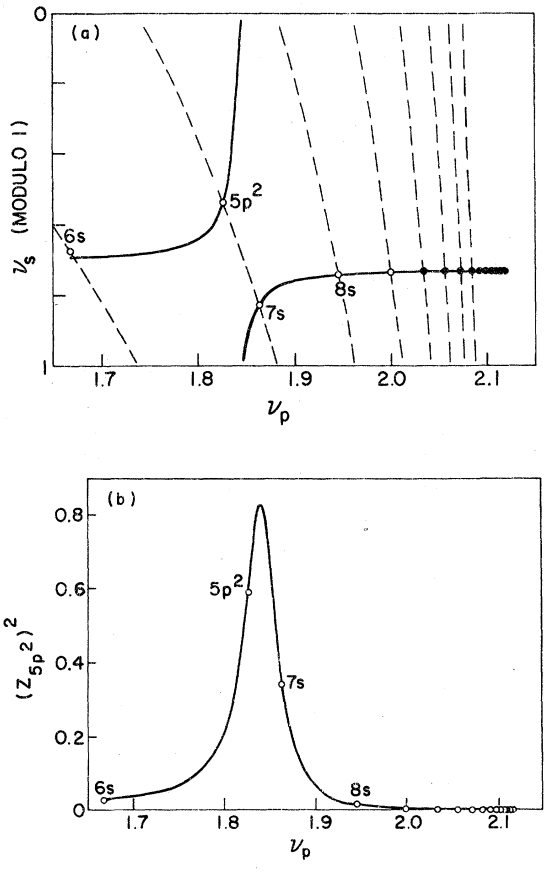

FIG. 4. (a) Quantum-defect plot of the $^1S_0$ bound states. The symbols are ○ for previously observed (Ref. 5) states and ● for the new data (Table III). The solid curve $\mathcal{S}$ is given by solving Eq. (3) for ν_s with the parameters given in Table VI. The dashed line is $\mathcal{L}$ [Eq. (1)] with $I_s = 45\,932.14$ and $I_p = 70\,048.00$ cm^{-1} for the ionization limits. (b) Admixture of the $5p^2$ configuration in the bound $^1S_0$ series, calculated from Eq. (4) with the parameters in Table VI.

A quantum-defect plot of the $^1S_0$ states is shown in Fig. 4(a). The open circles correspond to the previously observed $^1S_0$ states,[5] and the filled circles correspond to the new data (Table III). The configuration which perturbs the $5sns$ series is the $5p^2$ member of the $5pnp$ series. Thus, the horizontal axis (ν_p) of this plot is computed from Eq. (1) using $I_i = I_p = 70\,048$ cm^{-1}, the average of the spin-orbit split $5p$ $^2P_{1/2}$ and $^2P_{3/2}$ limits.

The majority of the data points in Fig. 4(a), those above $5s7s$, lie near a horizontal line (constant ν_s, modulo 1), corresponding to nearly pure $5sns$ configurations. Two lower-energy states, labeled $5p^2$ and $5s7s$ from Ref. 5, deviate from this behavior because of the doubly excited state. The solid line in Fig. 4(a), which corresponds to the solution $\mathcal{S}$ of Eq. (2) using the least-squares-fit MQDT parameters (given in Table VI) for this data, is seen to fit the $5p^2$ perturbation quite accurately.

The calculated term values occur at the intersection of the solid curve $\mathcal{S}$ and the dashed curve $\mathcal{L}$ [Eq. (1)] in Fig. 4(a). As was true for Ca,[2] the MQDT model is unable to accurately fit the lowest energy excited $^1S_0$, $5s6s$ in Sr, even with a linear energy dependence of the μ_1 eigendefect. The energy of this state is strongly effected by polarization of the ion core by the outer electron and thus, it is not easily treated by MQDT. For this reason, it was omitted from the least-squares fit. The estimated error for each data point was used to appropriately weight the least-squares fit. Term values from Ref. 5 were assigned an es-

TABLE VI. MQDT parameters for the $^1S_0$ bound states.

$i, \alpha = 1$	2
$\lvert i\rangle = 5sns$	$5pnp$
$I_i = 45\,932.19$	70 048.11
$\mu_\alpha = 0.2907(6)$ [a]	0.1418(2)
$\frac{d\mu_\alpha}{dE} = 0.070(8)$ [b]	0
$U_{1\alpha} = 0.9366(6)$	−0.350(2)

[a] Probable error in last digit shown in parentheses.

[b] Normalized to energy from ground state to first (I_s) limit.

timated error corresponding to an uncertainty of 0.001 in ν_s. Term values calculated from the weighted least-squares-fit parameters appear in Table III. The weighted rms error between the observed and calculated values is 0.11 cm^{-1}.

The $(Z_{5p^2})^2$ admixtures for the $^1S_0$ series are plotted in Fig. 4(b). The doubly excited configuration is predominantly mixed into only two states, with the strongest admixture, 60%, occurring in the state conventionally labeled[5] $5p^2$. The sum of $(Z_{5p^2})^2$ over all bound $^1S_0$ states, excluding the $5s^2$ ground state, is 0.99.

D. Analysis of the even-parity $J = 2$ spectrum

The even-parity $J=2$ spectrum of Sr is by far the most complex of those discussed here. Figure 5 is a quantum-defect plot of the $J=2$ states, where the open circles correspond to previously observed states and the filled circles correspond to the new data (Table IV). This plot is a projection[2] of the four limit, and thus four dimensional, problem onto the ν_s and $\nu_{d\,3/2}$ axes. The coordinates (plotted modulo 1) along these axes, for a given energy E, are obtained from Eq. 1(b) (with $I_1=I_s=45\,932.19$ and $I_2=I_{D\,3/2}=60\,488.09$ cm^{-1}). The solid line in this figure passes through members of the Rydberg series which, below about $5s15d$, can be labeled $^1D_2$, whereas the broken line passes through members of the series which can be labeled $^3D_2$. An avoided crossing of the two series occurs near $5s15d$ and $5s16d$, and above this point the $^1D_2$ and $^3D_2$ labels of the curves should be reversed.

The quantum-defect plot (Fig. 5) of the newly obtained data (Table IV) shows that, in addition to the perturbation of the $5snd$ $^1D_2$ Rydberg series by a $5p^2$ term,[6] the $5snd$ $^1D_2$ and $^3D_2$ series are strongly perturbed by $^1D_2$ and $^3D_2$ terms of the $4d6s$ configuration. Further, as shown by the avoided crossing of the $^1D_2$ and $^3D_2$ series, there is clearly a breakdown of strict LS coupling of these Rydberg series. In this section, a five-channel MQDT model will be described which accurately reproduces all of these features. An extension of this model, which reproduces the observed $J=2$ autoionizing resonance, will also be discussed.

The first and most important step in an MQDT analysis is the identification of the relevant channels. In the MQDT analysis[2] of Ca, it was found that the bound, even-parity $J=2$ spectrum could be adequately treated assuming that both the (α) eigenchannels and the (i) collision channels were LS coupled, i.e., that $^1D_2$ and $^3D_2$ channels did not mix. However, it is clear, after considering Figs. 1 and 5, that LS coupling does not hold

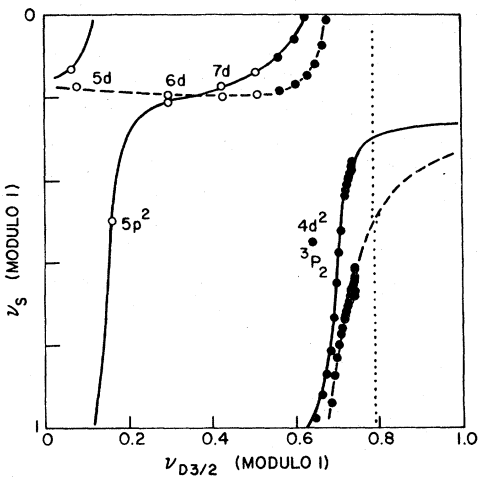

FIG. 5. Quantum-defect plot of the $J=2$ bound states. Symbols are ○ for previously observed states and ● for the new data (Table IV). The solid and broken curves correspond to the five-channel MQDT fit with the parameters given in Table VII. The solid line passes through members of the Rydberg series which, below $5s15d$, can be labeled $^1D_2$, whereas the broken line passes through members of the series which can be labeled $^3D_2$. Above $5s16d$, these labels are reversed. The dotted curve is the additional branch introduced by a six-channel model which also fits the observed $J=2$ autoionizing resonance near 46 380 cm^{-1}.

throughout the corresponding spectrum of Sr. Thus, for Sr, we must include the effects of spin-orbit coupling, manifested in the (280 cm^{-1}) spin-orbit splitting of the $(4d\ ^2D)$ ionization limits, and explicitly treat the recoupling problem using appropriately (jj) coupled collision channels. It will still be found, however, that configuration interactions are the largest perturbing influence on the $5snd$ series.

The (α) eigenchannels, found by fitting the observed data, are still expected to be very nearly LS coupled. Following Ref. 9, an intermediate basis $\bar{\alpha}$ of exactly LS coupled channels, with pure configurations, is introduced by factoring the $U_{i\alpha}$ transformation into the form

$$U_{i\alpha}=\sum_{\bar{\alpha}} R_{i\bar{\alpha}} V_{\bar{\alpha}\alpha}\,. \tag{5}$$

The pure configurations of the (i) collision channels are preserved in the $(\bar{\alpha})$ intermediate channels by maintaining the $R_{i\bar{\alpha}}$ matrix in a block diagonal form. Each block along the diagonal is then simply given by the known[10] $(jj\,|\,LS)$ recoupling matrix. If we have correctly assumed that the LS coupling labels of the $\bar{\alpha}$ channels also apply to the α eigenchannels, then the V matrix in

Eq. (5) should only couple terms of the same L and S from different configurations.

The identification of the relevant channels for the bound even-parity $J=2$ spectrum proceeds as follows: The two principal channels are the $^1D_2$ and $^3D_2$ Rydberg series of the $5snd$ configuration, which converge on the $5s\ ^2S_{1/2}$ ionization limit. In addition to these two singly excited series, there are Rydberg series of doubly excited configurations converging on higher limits. Only those series converging on limits associated with the lower energy excited states ($4d$ and $5p$) of the ion are important, provided we limit ourselves to the energy region of the bound states. Thus, we look for $J=2$ channels arising from even-parity configurations involving either $4d$ or $5p$ core excitations. This leads to a set of eight "perturbing" channels with the $\bar{\alpha}$ (LS coupled) labels $4d6s$ ($4dns$) $^1D_2$ and $^3D_2$; $4d^2$ ($4dnd$) $^3P_2$, $^1D_2$, $^3F_2$, and $5p^2$ ($5pnp$) $^3P_2$, $^1D_2$, and $^3F_2$.

Not all of the above channels are required to fit the known data of the bound $J=2$, even-parity spectrum. For an initial treatment of the bound spectrum it is found that all three channels from the $4d^2$ configuration can be ignored. Furthermore, since the only perturbations observed due to the $5p^2$ configuration are due to the $^1D_2$ term, the $^3P_2$ and $^3F_2$ terms of this configuration can also be ignored. We thus take as a starting point a basis set composed of the five channels with $^1D_2$ and $^3D_2$ labels in the $\bar{\alpha}$ intermediate basis. These five channels are explicitly listed at the top of Table VII. Note that by taking only the $^1D_2$ term of the $5pnp$ channel, only one value is required for I_p the $5p$ ionization limit. Thus, once again, we take I_p equal to the average of the spin-orbit split $5p\ ^2P_{1/2}$ and $^2P_{3/2}$ limits.

As a reasonable first step in the MQDT analysis, the model used did not introduce any mixing between the perturbing channels ($4dns$ and $5pnp$), other than the $R_{i\bar{\alpha}}$ recoupling within each configuration. Further, the V matrix was initially assumed to mix only $\bar{\alpha}$ channels with identical values of L and S, i.e., no configuration mixing was introduced between $^1D_2$ and $^3D_2$ channels.

Using this model, the μ_α and $V_{\bar{\alpha}\alpha}$ parameters were adjusted to obtain the best fit of the data. This task was greatly simplified by the use of a graphics display terminal and interactive computer programs. Initial values for the μ_α parameters could be estimated from appropriate[2] projections of the multidimensional four-limit quantum-defect plot. The data were then graphically compared with the theoretical curve δ obtained, for a given set of parameters, by solving Eq. (3) for ν_s with the remaining ν_i appearing in Eq. (3) given by Eq. (1). Parameters were then refined, first by trial and error adjustment, and finally by least-squares fitting. The data were weighted for the least-squares fit on the basis of

TABLE VII. MQDT parameters for even-parity $J=2$ bound states.

$i,\bar{\alpha},\alpha=$	1	2	3	4	5
$\lvert i\rangle$ =	$[^2S_{1/2}]d_{3/2}$	$[^2S_{1/2}]d_{3/2}$	$[^2D_{5/2}]s_{1/2}$	$[^2D_{3/2}]s_{1/2}$	$[^2P]p$
I_i =	45 932.19	45 932.19	60 768.43	60 488.09	70 048.11
$\lvert\bar{\alpha}\rangle$ =	$5snd\ ^1D_2$	$5snd\ ^3D_2$	$4dns\ ^1D_2$	$4dns\ ^3D_2$	$5pnp\ ^1D_2$
μ_α =	0.760(3)[a]	0.767(1)	0.2934(3)	0.3119(1)	0.1891(5)
$\frac{d\mu_\alpha}{dE}$ =	0.31(2)[b]	0.25(2)	0	0	0
$V_{\bar{\alpha}\alpha}=$	0.884(1)	0	−0.436(3)	−0.072(3)	−0.154(3)
	0	0.9733(2)	0.038(1)	−0.227(1)	0
	0.435(3)	0	0.885(6)	0.146(5)	−0.076(2)
	0	0.230(1)	−0.159(6)	0.9602(1)	0
	0.172(3)	0	0	0	0.9851(6)
$R_{i\bar{\alpha}}=$	$\sqrt{3/5}$	$\sqrt{2/5}$	0	0	0
	$-\sqrt{2/5}$	$\sqrt{3/5}$	0	0	0
	0	0	$\sqrt{3/5}$	$\sqrt{2/5}$	0
	0	0	$-\sqrt{2/5}$	$\sqrt{3/5}$	0
	0	0	0	0	1
$U_{i\alpha}=$	0.685(1)	0.6155(1)	−0.314(2)	−0.199(2)	−0.119(2)
	−0.559(1)	0.7539(2)	0.305(2)	−0.130(2)	0.098(2)
	0.337(2)	0.1453(6)	0.585(4)	0.721(4)	−0.059(1)
	−0.275(2)	0.1780(7)	−0.683(4)	0.651(4)	0.048(1)
	0.172(3)	0	0	0	0.9851(6)

[a] Probable error in last digit shown in parentheses.

[b] Normalized to energy from ground state to first (I_s) limit.

the estimated errors from the data plus a minimum error corresponding to $\Delta\nu_s = 0.001$.

The theoretical curve 8 corresponding to the best fit obtained using the above model is shown as a solid line in Fig. 5. The model is immediately seen to reproduce all of the major features in the quantum-defect plot of all $^1D_2$ and $^3D_2$ states above the $5s4d$ levels. A linear energy dependence in the eigendefects of the $5snd$ $^1D_2$ and $^3D_2$ channels is found to be essential to fitting the levels in the region $5s5d$-$5s8d$. However, even with these additional parameters, forcing the theory to fit the $5s5d$ levels accurately leads to some sacrifice in the accuracy of the fit for the remainder of the levels.

The complete set of MQDT parameters obtained from the least-squares fit of the $J=2$ states is given in Table VII. Note, in $V_{\bar{\alpha}\alpha}$, that a weak coupling has been introduced between the $4dns$ $^1D_2$ and $^3D_2$ $\bar{\alpha}$ intermediate basis channels. This corresponds to relaxing the restriction that the α close-coupled channels are exactly LS coupled. The introduction of this weak coupling was found to significantly improve the least-squares fit in the region of the avoided crossing of the $^1D_2$ and $^3D_2$ series.

As discussed in Ref. 2, not all of the relative signs of the $V_{\bar{\alpha}\alpha}$ matrix, as shown in Table VII, are significant. The matrix shown was generated by successive rotations about different axes following the convention described in the appendix of Ref. 9. The sign of each rotation angle was arbitrarily chosen to be positive, except for that rotation which mixed the $4d6s$ $^1D_2$ and $^3D_2$ channels; the appropriate phase of this angle was determined by the phase convention used in forming the recoupling matrix. The four mixing angles which generate the $V_{i\bar{\alpha}}$ in Table VII are 0.457(3) and 0.172(3) rad for the $5snd$ $^1D_2$ mixing with $4dns$ and $5pnp$ $^1D_2$; 0.232(1) rad for the $4snd$ $^3D_2$-$4dns$ $^3D_2$ mixing; and $-0.164(5)$ rad for the $4d6s$ $^1D_2$-$^3D_2$ mixing. (The statistical estimate of the error in the last digit is shown in parentheses.) The theoretical term values calculated from this set of parameters are given in Table IV. The weighted rms deviations between the calculated and experimental values is 0.14 cm^{-1}.

The admixture Z_i^2 of each (i) configuration present in each of the bound states can be obtained from the best fit parameters using Eq. (4). Since the bound states of Sr are best described in terms of LS coupling, the $R_{i\bar{\alpha}}$ matrix can be used to transform the Z_i coefficients of the jj-coupled i basis into the $\bar{\alpha}$ basis, i.e.,

$$Z_{\bar{\alpha}} = \sum_i Z_i R_{i\bar{\alpha}} \ . \qquad (6)$$

These $Z_{\bar{\alpha}}$ coefficients correspond to LS coupled, pure configurations of the $\bar{\alpha}$ intermediate basis set. Using the MQDT parameters in Table VII, all of the bound states above the $5p^2$ $^1D_2$ level are found to be primarily (over 90%) admixtures of $5snd$ $^1D_2$ and $^3D_2$ channels. The separation of the bound state into a $^1D_2$ and a $^3D_2$ series is found to be valid except in the region from $5s13d$ to $5s19d$. This is shown in Fig. 6(a), which is a plot of the admixture of the $5snd$ $^1D_2$ channel in each state above $5s8d$. Members of the series labeled (below the $5s15d$ levels) by $^1D_2$ and $^3D_2$ are identified, as in Fig. 5, by solid and broken curves, respectively. The two curves clearly show the crossover of the "$^1D_2$" series into a "$^3D_2$" series, and vice versa, as one proceeds from below $5s15d$ up to and above $5s16d$. Since only the $^1D_2$ states carry appreciable intensity in the two-photon transitions from the $^1S_0$ ground state, these curves closely resemble the intensity pattern observed in Fig. 1. Referring to Fig. 1, note that the crossover in intensity (where the higher energy peak in each pair becomes, for the first time, the more intense peak) occurs between $5s15d$ and $5s16d$, at precisely the same point where Fig. 6(a) shows the two series reverse their "$^1D_2$" and "$^3D_2$" character.

The admixtures of the perturbing configurations $5p^2$ and $4d6s$ can also be obtained in the same manner. The state at 36960.9 cm^{-1} is found to have a 75% admixture of the $5p^2$ $^1D_2$ configuration, in agreement with the label given in Ref. 5. The admixtures of the $4d6s$ $^1D_2$ and $^3D_2$ configurations are found to be spread out over many of the $J=2$ bound states. No individual state is found with more than a 5% admixture of the $4d6s$ $^1D_2$ configuration or an 8% admixture of the $4d6s$ $^3D_2$ configuration, and thus no individual state can be appropriately given either of these labels. Figures 6(b) and 6(c) are plots of the admixtures, normalized per unit energy, of these two configurations that illustrate the rough position in energy of these two perturbing configurations. Note that the avoided crossing between the $^1D_2$ and $^3D_2$ series occurs in the midst of the $4d6s$ configuration interactions. This is not coincidental, but is a result of the different strengths of the interactions of the $^1D_2$ and $^3D_2$ $4d6s$ terms with the $^1D_2$ and $^3D_2$ $5snd$ series, respectively, which lead to the tendency of these curves to cross. Thus the admixture curves for $^1D_2$ and $^3D_2$ series in Sr are considerably more complex than in Ca, where $^1D_2$ and $^3D_2$ series could be treated separately.

There remains the problem of identifying, and if possible fitting to theory, the autoionizing resonance observed at 46380 cm^{-1}, just above the I_s limit. It is a simple matter to add an additional

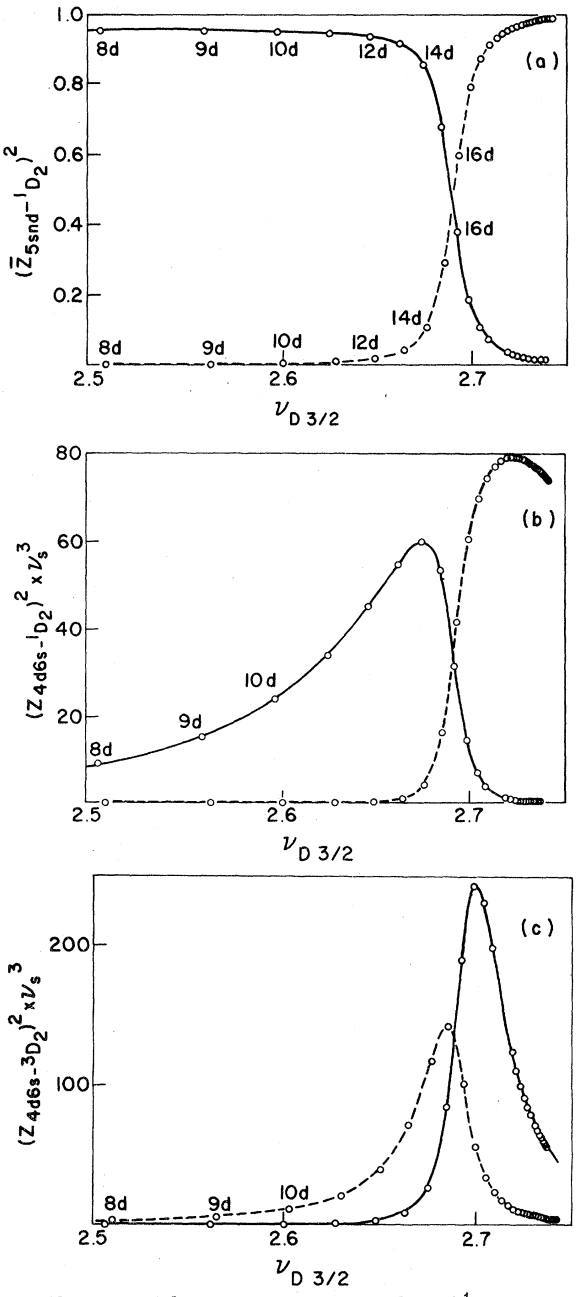

FIG. 6. (a) Admixture, per state, of 5snd $^1D_2$ configurations in the two principal bound $J=2$ series. The solid line passes through members of the Rydberg series which, below $5s15d$, can be labeled $^1D_2$, whereas the broken line passes through members of the series which can be labeled $^3D_2$. Above $5s16d$ these labels are reversed. (b) Admixture, per unit energy, of the $4d6s$ $^1D_2$ configuration in the two $J=2$ series. Solid and broken lines as above. The peak admixture, per state, of 4.6% occurs in the $5s11d$ $^1D_2$ level. (c) Admixture, per unit energy, of the $4d6s$ $^3D_2$ configuration in the two $J=2$ series. Solid and broken lines as above. The peak admixture, per state, of 7.8% occurs in the $5s17d$ $^3D_2$ level.

channel with an eigendefect chosen to match the observed autoionizing resonance. For the purpose of choosing this eigendefect, we *assume* the new channel converges on the $4d\ ^2D_{3/2}$ limit. (The validity of this choice can only be determined with additional autoionizing spectra.) The width of the resonance is directly related to the elements of $U_{i\alpha}$ which describe the strength of interaction between this new channel and the underlying continuum channels.

The intensity of the multiphoton ionization signal versus E is shown by the points plotted in Fig. 7. Although conversion from the log scale of Fig. 1 to a linear scale diminishes the apparent asymmetry of the resonance, it is clear that a fit of this line shape must include the interference between the transition strengths of the continuum and of the autoionizing state.

In order to calculate intensities in the autoionization spectrum, a set of dipole matrix elements,[9] $D_{\bar{\alpha}}$, must be introduced to describe the inherent oscillator strength for each channel. One can assume that two of the $D_{\bar{\alpha}}$, corresponding to the $^3D_2$ channels are zero, and that a third $D_{\bar{\alpha}}$, corresponding to the far removed $5p^2\ ^1D_2$ channel, is also zero. The solid curve in Fig. 7 corresponds to the best fit obtained by adjusting three values of $D_{\bar{\alpha}}$ (for the $5snd$, $4dns$, and $4dnd$ $^1D_2$ channels), the eigendefect of the sixth channel, and the mixing of the sixth channel with the $5snd$ $^1D_2$ continuum. The MQDT parameters for the remaining five channels were identical to those used in the previous fit of the bound-state energies. The intensity fit is seen to be quite good. The deviation between the calculated and observed intensities is probably caused by experimental errors, such as saturation of the ion signal (see Ref. 2). Errors of this type are not expected to significantly alter the overall features of the MQDT fit.

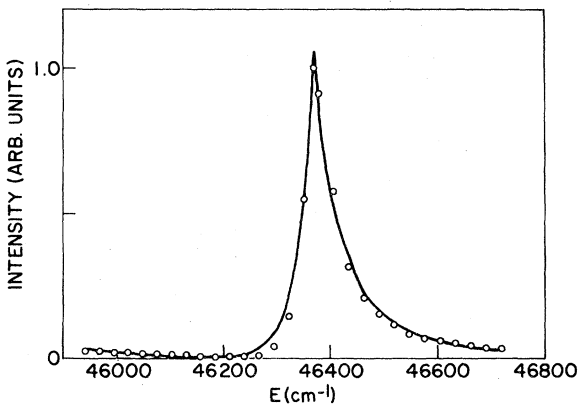

FIG. 7. Intensity of observed autoionizing resonance (points) and MQDT fit (solid line) of this data.

The quantum-defect plot corresponding to the six-channel MQDT model, which fits the autoionizing resonance, is shown as a dotted curve in Fig. 5. The addition of the sixth channel does not significantly alter the fit of the bound states. This is a consequence of the sharpness of the resonance, i.e., the weakness of interaction, corresponding to this channel.

Returning to the MQDT fit of the $J=2$ bound states, the largest variance (with respect to estimated experimental errors) between theoretical and experimental term values occurs for the $^1D_2$ states just above and below the energy of the $4d^2\ ^3P_2$ term at 44729.7 cm^{-1}. This is the only evidence, in the bound-state region, for a perturbation due to the $4d^2$ configuration. Note that only the $^1D_2$ terms, and not the $^3D_2$ terms, are perturbed by the $^3P_2$ state. This may be understood by realizing that the perturbation can only occur if there is a breakdown of the LS coupling of the $4d^2$ state, which would mix the $^3P_2$, $^1D_2$, and $^3F_2$ terms of this configuration. Assuming some configuration interaction mixes the $4d^2\ ^1D_2$ with the primary $^1D_2$ series, this provides a mechanism for the $^3P_2$ state to interact with the $^1D_2$ series. Since there is no $^3D_2$ term of the $4d^2$ configuration, interactions between $^3P_2$ and $^3D_2$ terms can occur only in an even higher order.

Since the observed perturbations of the $^1D_2$ series by the $4d^2\ ^3P_2$ state are linked to the interactions of the $4d^2\ ^1D_2$ channel, an eight-channel MQDT treatment of the bound $J=2$ spectrum was attempted. The six-channel model used to fit the observed autoionizing resonance was expanded to also include $4d^2\ ^3P_2$ and $^3F_2$ channels. Recoupling between the three $4d^2$ terms was given by appropriate $(jj\,|\,LS)$ matrix,[10] and both $^2D_{3/2}$ and $^2D_{5/2}$ limits were utilized. Since no $4d^2\ ^3F_2$ state has been observed, μ_α for this channel was arbitrarily chosen as zero, whereas μ_α for the $^3P_2$ and $^1D_2$ channels were well defined by the respective energies of the $^3P_2$ state and the autoionizing resonance. However, this model was not able to simultaneously fit the observed perturbation between the $^1D_2$ and $^3P_2$ bound states as well as the observed width of the autoionizing resonance. The strong mixing between the $4d^2\ ^1D_2$ and $5snd\ ^1D_2$ channels necessary to reproduce the $^3P_2$ perturbations leads to the prediction of a much larger width autoionizing resonance than the observed resonance.

E. Discussion

In the preceding section, we have shown that MQDT parametrizations are capable of accurately reproducing the $^1S_0$, $^1P_1^o$, $^1D_2$, and $^3D_2$ bound-state spectra of Sr. We have also demonstrated that the intensity profile of the observed $J=2$ autoionizing resonance (at 46380 cm^{-1}) can be fit by a simple extension of the MQDT model used to fit the $J=2$ bound-state energies. However, the exact assignment of the configuration responsible for this autoionizing resonance still remains in question.

A comparison of the MQDT analyses of the $J=2$, even-parity spectra of Ca and Sr initially leads to the assignment of the 46380 cm^{-1} autoionizing resonance in Sr to the $4d^2\ ^1D_2$ configuration. However, a more detailed consideration of such an assignment uncovers inconsistencies, arising from the narrow width observed for this resonance, which leads us to question the above assignment.

The first inconsistency, discussed in the previous section, was the inability to simultaneously fit the observed perturbation between $5snd\ ^1D_2$ and $4d^2\ ^3P_2$ states as well as the observed width of the autoionizing resonance.

A second inconsistency can be found in Table VIII, where the MQDT parametrizations of the $^1S_0$, $^1P_1^o$, $^1D_2$, and $^3D_2$ series of Ca and Sr are compared. For the most part, there is a strong correlation, in Table VIII, between the parameters obtained for Sr and those obtained[2] for Ca. However, this correlation clearly breaks down for the two

TABLE VIII. Comparison of MQDT parameters obtained for Ca and Sr.

		Ca (Ref. 2)	Sr
$^1S_0$	μ_{ss} [a]	$0.347+0.07dE$ [b]	$0.291+0.07dE$
	μ_{pp}	0.172	0.142
	U_{pp-ss}	0.23	0.35
$^1P_1^o$	μ_{sp}	$0.968+0.19dE$	$0.894+0.25dE$
	μ_{dp}	0.566	0.491
	U_{dp-sp}	0.56	0.58
$^1D_2$ [c]	μ_{sd}	$0.801+0.44dE$	$0.760+0.31dE$
	μ_{ds}	0.336	0.293
	μ_{dd}	0.184	(0.211) [d]
	μ_{pp}	0.213	0.189
	V_{ds-sd}	0.42	0.44
	V_{dd-sd}	0.33	(0.036) [d]
	V_{pp-sd}	0.24	0.17
$^3D_2$ [c]	μ_{sd}	$0.870+0.18dE$	$0.767+0.25dE$
	μ_{ds}	0.339	0.312
	V_{ds-sd}	0.27	0.23

[a] Indices corresponding to α channels have been given approximate labels, corresponding to the α basis.

[b] Energy-dependent eigendefect, where $dE=(I_s-E)/I_s$.

[c] Care should be taken in comparing MQDT parameters for $^1D_2$ and $^3D_2$ series in Ca and Sr since recoupling of these series has only been included for the Sr case.

[d] Parameters obtained assuming $4d^2\ ^1D_2$ assignment of the 46380 cm^{-1} autoionizing resonance.

parameters obtained for Sr by fitting the 46 380 cm^{-1} autoionizing resonance, if we assume that this resonance is due to the $4d^2\ ^1D_2$ channel. For example, the magnitude of the $V_{dd\text{-}sd}$ matrix element which fits the observed width of this resonance is roughly ten times smaller than the magnitude of the corresponding element found for the $3d^2\ ^1D_2$ channel in Ca. Furthermore, whereas all other eigendefects in Sr are between 0.03 and 0.1 smaller than the corresponding eigendefects in Ca, the eigendefect U_{dd} which fits the energy of the autoionizing resonance in Sr is 0.03 *larger* than the $3d^2\ ^1D_2$ eigendefect in Ca.

In the face of these inconsistencies, a conclusive assignment of this $J=2$ autoionizing resonance will have to await additional data on the even-parity autoionizing spectrum.

Note added in proof. Many of the experimental results I have presented here have also been presented in a recent paper by Ewart and Purdie.[11] In their spectra, also obtained via multiphoton ionization, the $5d10d\ ^1D_2$ level (which appears weakly in our spectra) and the $5s12d$ to $5s24d\ ^3D_2$ levels are not identified. Without these levels, analysis of their data was hampered, and the details of the avoided crossing of the $^1D_2$ and $^3D_2$ series are missed entirely.

The MQDT treatment of the bound $^1P_1^o$ series, given here in Sec. IV B, has recently been published independently by K. T. Lu.[12] The results given here are in complete agreement with Dr. Lu's study,[12] which also attempted to fit the width of the $4d6p\ ^1P_1^o$ autoionizing resonance on the basis of the MQDT fit of the bound-state spectrum. I would like to thank Dr. K. T. Lu for bringing the above two papers to my attention.

Finally, we have recently studied the $5snp\ ^3P^o$ series of Sr and found that the $5s22p \rightarrow 5s33p\ ^3P_1^o$ term values given by Garton and Codling[7] differed from our results.[13] Garton[14] suggested that the states identified as $^3P_1^o$ in Ref. 7 were in reality transitions to even parity states. On comparison of their term values to the term values presented in this paper, one concludes that the states observed by Garton and Codling were the $5s20d$ to $5s31d\ ^1D_2$ states (Table IV). These states presumably appeared in their absorption spectra via quadrupole transitions from the $^1S_0$ ground state.

ACKNOWLEDGMENTS

The author would like to express his gratitude to Dr. J. A. Armstrong and to Dr. J. J. Wynne for their continuing discussions and critical readings of this paper, in addition to their overall support of this work. Appreciation is also expressed to L. H. Manganaro for his able technical assistance in the experimental work.

---

†Supported in part by the U.S. Army Research Office.

[1]P. Esherick, J. A. Armstrong, R. W. Dreyfus, and J. J. Wynne, Phys. Rev. Lett. 36, 1296 (1976).
[2]J. A. Armstrong, P. Esherick, and J. J. Wynne, Phys. Rev. A 15, 180 (1977).
[3]M. J. Seaton, Proc. Phys. Soc. (London) 88, 801 (1966).
[4]U. Fano, J. Opt. Soc. Am. 65, 979 (1975).
[5]C. E. Moore, *Atomic Energy Levels*, NBS Circ. No. 467 (U.S. GPO, Washington, D.C., 1952), Vol. 2.
[6]K. T. Lu, J. Opt. Soc. Am. 64, 706 (1974).
[7]W. R. S. Garton and K. Codling, J. Phys. B 1, 106 (1968).
[8]K. T. Lu, Phys. Rev. A 4, 579 (1971).
[9]C. M. Lee and K. T. Lu, Phys. Rev. A 8, 1241 (1973).
[10]E. U. Condon and G. H. Shortley, *The Theory of Atomic Spectra* (Cambridge U.P., Cambridge, 1957), p. 294.
[11]P. Ewart and A. F. Purdie, J. Phys. B 9, L437 (1976).
[12]K. T. Lu, Proc. R. Soc. Lond. (to be published).
[13]P. Esherick, J. J. Wynne, and J. A. Armstrong (to be published).
[14]W. R. S. Garton (private communication).